Chapter 29
From the Initial to the Present Sun

There is evidence on Earth that the Sun has shone for more than 3,000 million years with about the same luminosity. From radioactive decay in different materials of the solar system, one nowadays assumes that it was formed 4.57 Gigayears (Gyrs; 10^9 years) ago. Since then, the Sun has lived on hydrogen burning, predominantly according to the *pp* chain, and its interior has been appreciably enriched in ^{4}He. In the following we show how a model of the present Sun can be constructed.

29.1 Known Solar Data

Although the Sun is a very ordinary star of average mass and in a quiet state of main-sequence hydrogen burning, it is a unique object for stellar evolution theorists. For no other star so many quantities are known with comparable accuracy obtained by so many different and independent methods. From Kepler's laws and known distances within the solar system we can derive its mass and radius as well as the total luminosity. This yields the effective temperature by application of the Stefan-Boltzmann law. Neutrino experiments on Earth (see Sect. 29.5) allow the determination of conditions in the innermost energy producing core. And the art of (helio-)seismology has returned with high accuracy the run of the sound speed throughout most of the solar interior, the helium content of the outer convective envelope, and its depth. These quantities restrict the modelling of the present Sun and allow a comparison with stellar evolution theory at a degree of precision which is almost unique in astrophysics. Table 29.1 summarizes the fundamental solar parameters and the method to derive them. Note that the rather large uncertainty in the solar mass is the result of the uncertainty in Newton's constant of gravity G. Kepler's third law returns their combination, $GM_\odot$, with a precision of 10^{-7}!

There is still one significant uncertainty in the solar quantities, and this is the present surface (or convective envelope) composition. The determination by Grevesse and Noels (1993) was considered to be very close to the real composition, as it also agreed very well with meteoritic values in those elements

R. Kippenhahn et al., *Stellar Structure and Evolution*, Astronomy and Astrophysics Library, DOI 10.1007/978-3-642-30304-3_29,

Table 29.1 Solar quantities and how they are derived

Quantity	Value	Method
Mass	$(1.9891 \pm 0.0004) \times 10^{33}$ g	Kepler's third law
Radius	$695,508 \pm 26$ km	Angular diameter plus distance
Luminosity	$(3.846 \pm 0.01) \times 10^{33}$ erg s^{-1}	Solar constant
Effective temp.	$5,779 \pm 2$ K	Stefan-Boltzmann law
Z/X	0.0245 ± 0.001	Meteorites and solar spectrum
	0.0165	(new determination)
Age	4.57 ± 0.02 Gyr	Radioactive decay in meteorites
Depth of conv. env.	$0.713 \pm 0.001\ R_\odot$	Helioseismology
Env. helium content	0.246 ± 0.002	Helioseismology

(Z/X) is given twice: the more traditional value by Grevesse and Noels (1993) and the more recent one by Asplund et al. (2005)

that can be compared. However, new analyses of the solar spectrum (Asplund et al. 2005, 2009), done with sophisticated three-dimensional, non-LTE radiation-hydrodynamics methods, returned (see Table 29.2) much lower values in particular for the volatile elements C, N, and O, which cannot be measured accurately in meteorites. The difference is a reduction of the total amount of metals relative to hydrogen, (Z/X), by 30 %! The latest revision by Asplund et al. (2009) for the solar element composition resulted in somewhat higher abundances than the 2005 values but still distinctively lower than the Grevesse and Noels numbers. Consequently, the structure of solar models using the 2009 abundances lies between the two other cases, which we will present in the following. This issue is not yet settled, but since the solar composition is the yardstick for all abundance determinations in astrophysics, the outcome will certainly be of great importance.

As we will see, the older abundance data yielded solar models in very good agreement with helioseismology. The lower abundances deteriorate this. In the following we will present a standard solar model based on the older Grevesse and Noels (1993) abundances, since such a model appears to be closer to the real solar structure, even if this could be due to coincidence.

A *standard solar model* is derived under the assumptions of spherical symmetry and hydrostatic equilibrium, ignoring effects of rotation and the influence of magnetic fields. Convection is usually treated in mixing-length theory, and no overshooting is assumed. The only effect beyond these most basic assumptions is the inclusion of atomic diffusion, since it turned out that models which disregarded this disagree more with seismic results. This is true for both sets of solar abundances mentioned above.

A solar model has to match the solar radius, luminosity, and surface abundance of metals at the solar age. The evolution is started from the pre-main-sequence hydrostatic contraction until the solar age. The mass can be kept fixed because mass loss is known to be unimportant.

Table 29.2 Solar atmospheric and meteoritic abundances of the most important elements, as determined by Grevesse and Noels (1993; "GN93") and Asplund et al. (2005, "AGS05")

Element	GN93	AGS05	Meteorites
H	12.00	12.00	8.25
C	8.55	8.39	7.40
N	7.97	7.78	6.25
O	8.87	8.66	8.39
Ne	8.08	7.84	−1.06
Na	6.33	6.17	6.27
Mg	7.58	7.53	7.53
Al	6.47	6.37	6.43
Si	7.55	7.51	7.51
S	7.21	7.14	7.16
Cl	5.50	5.50	5.23
Ar	6.52	6.18	−0.45
Ca	6.36	6.31	6.29
Ti	5.02	4.90	4.89
Cr	5.67	5.64	5.63
Mn	5.39	5.39	5.47
Fe	7.50	7.45	7.45
Ni	6.25	6.23	6.19
Z/X	0.0245	0.0165	

Abundances are given in logarithms of particle abundance on a scale on which hydrogen has the abundance of 10^{12}

The abundance of helium cannot be determined from the spectrum and is therefore missing

Errors are for most elements in the range of 0.02–0.06 dex

Neon and argon can be determined only indirectly from coronal abundance ratios with respect to oxygen, and are basically absent in meteorites

The bottom line gives the total metallicity in mass fractions relative to hydrogen

29.2 Choosing the Initial Model

While the observations yield information about the mass abundance Z of heavier elements, it is difficult to determine spectroscopically the helium content Y of the solar surface. One therefore uses Y as a free parameter. This is actually the initial helium content Y_i, which will change during the evolution due to the effects of nuclear burning and diffusion. Its value cannot be compared directly with an observed value. Sedimentation–the main effect of diffusion–will also lead to a reduction of Z/X with time. Therefore also the initial metallicity Z_i has to be chosen such that after 4.57 Gyr the present Z/X is obtained. Furthermore, there is no information about the mixing length ℓ_m to be used in the convection theory (see Chap. 7). One normally expresses ℓ_m in units of the local pressure scale height H_P and treats the dimensionless quantity ℓ_m/H_P as another free parameter.

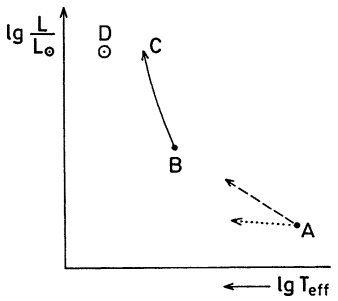

Fig. 29.1 Finding a model that for given values of $Z = 1 - X - Y$ describes the present Sun. For arbitrary values of Y, $\ell_{\rm m}$ one obtains a ZAMS model at A, from where it shifts along the *broken* and *dotted arrow* as a result of independent changes of Y and $\ell_{\rm m}$, respectively. Based on this, one guesses the values of Y, $\ell_{\rm m}$ that yield the model at B. Its evolution is calculated from age zero (B) to $t = 4.57 \times 10^9$ years (C). The guessed values Y, $\ell_{\rm m}$ are modified until C coincides with D (present Sun)

We now sketch the way to obtain a solar model using some simplifications. These are not done in numerical calculations, but they allow us to use properties of simplified models. We first ignore diffusion. Then $(Z/X)_{\rm i}$ is known from the present photospheric abundances. We now start the construction of an initial solar model with trial values of $Y_{\rm i}$ and $\ell_{\rm m}/H_P$. Since the model changes only on the (long) nuclear timescale, it can well be approximated by assuming complete equilibrium. This means that in addition to the inertia term in (10.2) the time derivatives in the energy equation (10.3) can be neglected. The evolution can then be followed from the ZAMS until a time of 4.57×10^9 years after the onset of hydrogen burning has elapsed. During this time interval the molecular weight in the central regions increases owing to the enrichment of helium. Consequently, the luminosity increases slightly, as can be expected from the homology relation (20.20) according to which the luminosity should increase like μ^4. (The fact that the solar evolution is not homologous changes the result only quantitatively.) At the same time, the point in the Hertzsprung–Russell (HR) diagram moves slightly to the left. If our choice of the free parameters were correct, the model after 4.57×10^9 years should resemble the present Sun. But, in general, this will not be the case, and the evolutionary track will miss the image point of the present Sun. One therefore has to adjust the two free parameters in order to end up with the present Sun.

A variation of the mixing length changes the radius slightly, but turns out to have almost no influence on the luminosity. Therefore, while varying $\ell_{\rm m}$, the initial model will move almost horizontally (Fig. 29.1). If, on the other hand, $Y_{\rm i}$ is changed, the mean molecular weight μ varies. With increasing helium content, μ also increases, and since the computed models roughly behave as the homologous models of Sect. 20.2.2, the image point of the model moves to the upper left on a line below the main sequence [see the arguments after (20.23)].

Since small changes in the two parameters do not modify the form of the evolutionary track very much, the whole track makes an approximately parallel

Table 29.3 Dependence of solar model quantities on model parameters

	ℓ_m/H_P	Y_i	Z_i
$L/L_\odot$	0.038	*8.515*	−38.60
$R/R_\odot$	*− 0.129*	2.019	−7.05
$(Z/X)/(Z/X)_\odot$	0.043	0.523	*56.0*

The table entries are to be read as the partial derivative of the column quantity with respect to the row quantity
The strongest influence by each parameter is in italics

shift. Therefore one can find values for Y_i and ℓ_m/H_P for which the end point of the evolutionary track coincides with the point of the (observed) present Sun. The procedure is illustrated in Fig. 29.1. A model constructed in this way, and by using the standard assumptions for the input physics, is often called a "standard solar model".

Table 29.3 gives an overview of the partial derivatives $\partial y/\partial x$ in the vicinity of the final, calibrated solar model, where y corresponds to the solar observable (rows) and x to the model parameter (columns). The values were obtained from the solar model calculations presented in the next section. While the absolute numbers depend a lot on the individual calculation, the relative ratios are very similar for all solar model calibrations. Clearly, the initial helium content affects mostly the luminosity and the mixing length the radius of the solar model. The initial metallicity Z_i has not only an obviously direct effect on Z/X but also, due to the change of μ, on luminosity.

The values of the initial Y and ℓ_m/H_P, which after 4.57×10^9 years lead to the present Sun, depend sensitively on the details of the computations, for instance, on the opacities used and the equation of state applied.

29.3 A Standard Solar Model

After the procedure to compute a standard solar model has been outlined, we now show the results of such a detailed computation. The final model agrees with the present solar luminosity and effective radius (Table 29.1) to 1 part in 10^4 or better and has $Z/X = 0.0245$ according to the analysis of Grevesse and Noels (1993), from which also the chemical composition (Table 29.2) was taken. The effect of diffusion was included. Up-to-date tables for the equation of state (Sect. 16.6) and the opacities (Sect. 17.8) were used, the latter for the same metal composition of Grevesse and Noels (1993). The calculation starts with a homogenous pre-main-sequence model, since the assumption of a homogenous ZAMS model in complete equilibrium would already be too inaccurate (see Sect. 28.2).

All modern stellar evolution codes using the same physical input data are able to produce a standard solar model that reproduces known properties of the Sun at a similar accuracy and agree very well with each other.

The evolution in the Hertzsprung-Russell diagram is shown in Fig. 29.2. It begins with a fully convective, contracting pre-main-sequence model. At an age of 1.7 Myr

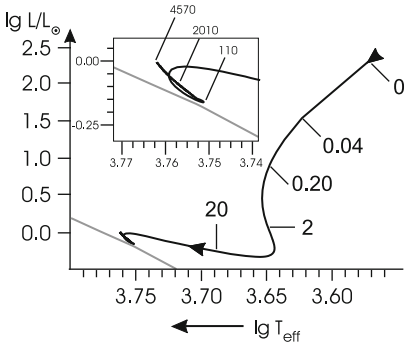

Fig. 29.2 Evolution of the standard solar model from the initial pre-main-sequence contraction to the present age. Ages in million years are indicated along the track. Notice the drastic slowdown of the evolution as soon as the nuclear timescale has become the dominant one and the rapid pre-main-sequence evolution on thermal timescales during the hydrostatic contraction along the Hayashi line. The main-sequence evolution and the phase immediately preceding it are magnified in the *inset* for clarity. The zero-age main sequence of Fig. 22.1 is shown as well. Since the solar composition is not exactly the same, the evolutionary path of the Sun is slightly offset from this ZAMS

the centre begins to become radiative; at that time $\log L/L_\odot$ has already dropped to 0.163. The evolution slows down considerably in the following. At 28.3 Myr and a luminosity of $\log L/L_\odot = -0.038$ and $\log T_{\rm eff} = 3.748$ a transient convective core begins to develop due to the strongly peaked energy release of the CN conversion. It lasts for about 120 Myr at which time the luminosity minimum has been reached. From there on the evolution proceeds on the very long nuclear timescale as the very short linear part of the track that ends at the solar position.

The initial homogeneous composition of this standard solar model is $X_{\rm i} = 0.7058$, $Y_{\rm i} = 0.2743$, and $Z_{\rm i} = 0.0199$. Z/X therefore was initially 0.0282 and has dropped at the photosphere to 0.0245 due to the settling of all heavier elements and the corresponding increase of hydrogen in the convective envelope. This effect is visible in Fig. 29.3, where the hydrogen and metal content X and Z as functions of m/M are plotted; the final surface hydrogen abundance is 0.7377 and that of metals 0.0181. They are higher, respectively lower than the initial ones because of the sedimentation of all elements heavier than hydrogen below the thin convective envelope. This leads to the sudden increase of hydrogen abundance to the higher and constant value in the convectively mixed outermost layers. Accordingly, the abundance of metals (dashed curve in Fig. 29.3) decreases at the beginning of the convective envelope.

In the central region of the present Sun, quite an appreciable percentage of the original hydrogen has already been converted into helium. The central value of X has dropped to 0.338. The abundance of ^{3}He, also shown in Fig. 29.4, displays the characteristic shape discussed in Sect. 28.2 due to its evolution towards an equilibrium value within the *pp* chain.

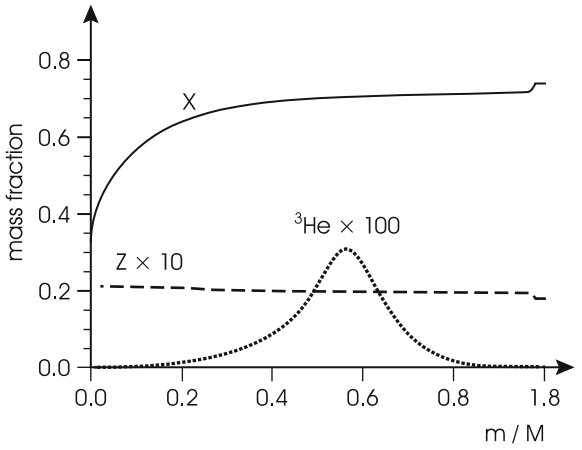

Fig. 29.3 Element abundances in a model for the present Sun (age 4.57×10^9 years) as a function of m/M. Shown are the mass fractions of hydrogen, (X, *solid line*), metals (Z, multiplied by a factor 10, *dashed line*), and of ^{3}He (multiplied by 100, *dotted line*). The initial values for X and Z in the homogeneous model were 0.7058, respectively 0.0199. The increase in X and the decrease in Z in the outermost regions is due to the effect of diffusion

Some details of the solar structure are shown in Fig. 29.4. The left panel shows the concentration of mass. More than 80 % are contained within 40 % of the solar radius or just 6.4 % of the volume. Temperature rises over two orders of magnitude within the outermost 20 % of the radius, but then only by another factor of ten until the centre. Pressure and density profiles have a similar shape like that of temperature. In the right panel the strongly peaked energy generation is shown, which results in the fact that over 90 % of the total luminosity are reached already at $r/R_\odot = 0.2$, corresponding to a mass coordinate of only 0.3. Note the similarity of the solar structure to that of the 1 $M_\odot$ ZAMS model of Fig. 22.4. Although the Sun has burnt hydrogen for almost 5 billion years, it still has the shape of a young star.

Had we used the abundances of Asplund et al. (2005; middle column in Table 29.2) with the corresponding present value for Z/X of 0.0165, the structure of that solar model would hardly be distinguishable from the one shown in Fig. 29.4. However, initial and present composition would be different: the initial abundances in that case are $X_\mathrm{i} = 0.7261$, $Y_\mathrm{i} = 0.2599$, and $Z_\mathrm{i} = 0.0140$, and the present solar surface values are $X = 0.7578$, $Y = 0.2297$, and $Z = 0.0125$.

The outer convective zone of our standard solar model reaches down to a temperature of 2.2×10^6 K. The radius of its inner boundary is $r = 0.713\ R_\odot$, and the corresponding mass is $0.9761\ M_\odot$.

The temperature gradients ∇, ∇_ad, and ∇_rad as defined in Chaps. 5–7 are plotted in Fig. 29.5. In the near-surface regions where $\lg P < 5.0$, one finds $\nabla_\mathrm{rad} < \nabla_\mathrm{ad}$ and the layer is stable (Fig. 29.5a). Then convection sets in where ∇_rad exceeds ∇_ad. In the outermost part of the convective zone the convection is very ineffective and ∇ is close to ∇_rad, according to the considerations in Sect. 7.3. But ∇ does not follow

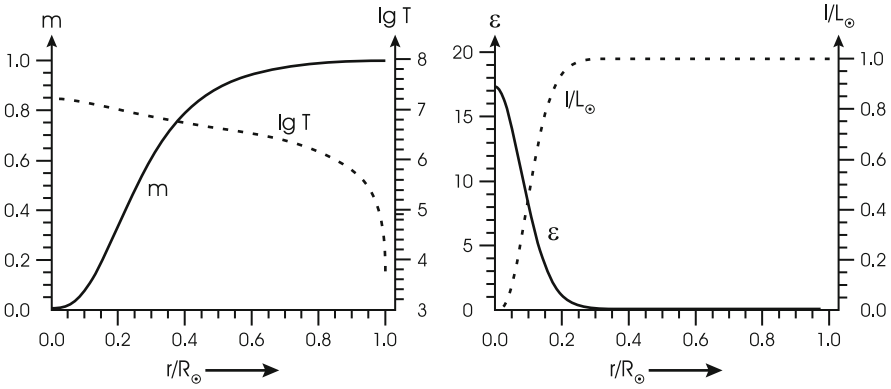

Fig. 29.4 Internal structure of the standard solar model as function of relative solar radius $r/R_\odot$

$\nabla_{\rm rad}$ to the extreme values (which at lg $P = 9$ reach a maximum of 4.1×10^5). It never exceeds 0.9. Owing to partial ionization of the most abundant elements, $\nabla_{\rm ad}$ is not constant in the outer region of the solar model, as we have already shown in Fig. 14.1b. The deeper inside, the more the actual gradient approaches the adiabatic one, following it up and down (Fig. 29.5a, b). In Fig. 29.5c the convective velocity obtained from U, $\nabla_{\rm rad}$, and ∇ according to (7.6) and (7.15) is given in units of the (isothermal) velocity of sound $v_{\rm s} = (\Re T/\mu)^{1/2}$. At the top of the convection zone, $v/v_{\rm s}$ reaches its maximum of about 0.4.

29.4 Results of Helioseismology

It is not surprising that one can produce models for the present Sun which have the correct position in the HR diagram, since three free parameters, $Y_{\rm i}$, $\ell_{\rm m}$ and $Z_{\rm i}$, can be varied to adjust the quantities L, R, and Z/X. Therefore obtaining a solar model with the right age at the right position in the HR diagram and the right surface composition is not much of a test of stellar evolution theory.

At present there are two observational tests to compare the solar interior with model calculations. One are solar neutrino experiments, which will be discussed in the next section. They test the conditions at the solar centre, where nuclear reactions take place. The other one allows an almost complete "view" of the solar interior and is based on the investigation of non-radial solar oscillations, commonly called helioseismology. We shall deal with such oscillations later (see Sect. 42.4). For the moment it is sufficient to state that the frequencies of thousands of non-radial solar oscillation modes, measured with extremely high precision, depend in particular on the sound speed profile throughout the Sun. In the following we discuss the most important results for the solar interior.

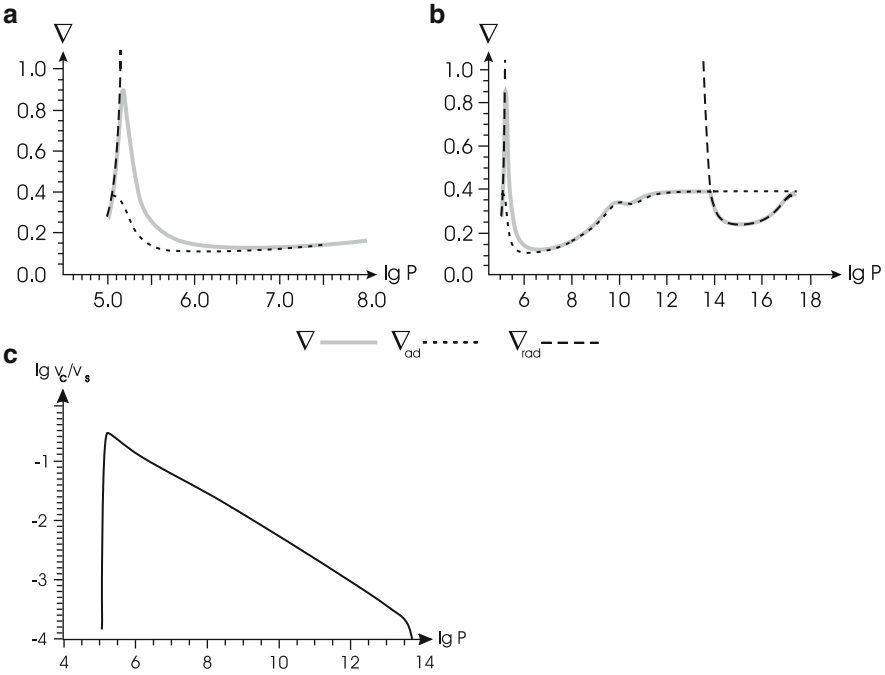

Fig. 29.5 Some properties of the model for the present Sun described in the text. (**a**) The temperature gradients in the outer layers, against the pressure P (in dyn cm^{-2}). In the outermost layers the actual gradient ∇ (*gray-shaded line*) coincides with $\nabla_{\rm rad}$ (*dashed line*), which then, however, goes up to values above the range of the ordinate. The strong depression of $\nabla_{\rm ad}$ (*lower short-dashed line*) for lg $P > 5$ is due to hydrogen ionization. (**b**) The same curves as in (**a**) but with compressed scales, such that the whole interior of the model is covered. $\nabla_{\rm rad}$ is still out of the range for almost all of the outer convective zone. The depression of $\nabla_{\rm ad}$ is caused by the ionization of H, He, and He^+ (at values of lg P around 6, 8, and 10). Note that the centre of the Sun is close to convective instability. (**c**) The convective velocity v in units of the local velocity of sound, $v_{\rm s}$, in the outer convective zone of the Sun

The first one is that the transition from the nearly adiabatic temperature gradient to the radiative one at the bottom of the convective zone leaves a significant change in the slope of the square of the sound speed divided by the gravitational acceleration (Gough 1986). This allows a very accurate determination of the bottom of the convective envelope, which is at $0.713 \pm 0.001\ R_\odot$. The solar model of Sect. 29.3 has exactly the same depth of the convective zone. The solar model with the newer abundance determination, in contrast, is convective to $0.731\ R_\odot$. This would favour the older abundances, provided that the physical input (equation of state, opacities, diffusion theory) is correct.

The second envelope quantity that can be determined by seismology is the envelope helium content and is based on the fact that the quantity Γ_1, defined in (13.18), depends on the chemical composition and therefore allows the determination of the helium abundance as the ionization of helium modifies Γ_1.

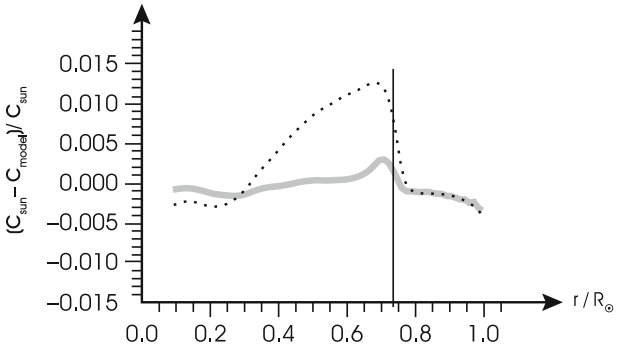

Fig. 29.6. The difference in sound speed c between that of the standard solar model computed in this chapter ("model") and that determined by helioseismology ("sun"; *grey shaded line*). Using the more recent abundance determination by Asplund et al. (2005) results in a larger difference (*dotted line*). The *vertical line* denotes the lower boundary of the convective envelope

The result is $Y = 0.246 \pm 0.005$, where for the error we have also considered possible systematic uncertainties. Again, the solar model with older abundances agrees with this value, having $Y = 0.244$, while the alternative model results in a lower value for helium of $Y = 0.230$.

Finally, the sound speed profile throughout most of the solar interior can be determined. The difference with respect to the standard solar model is shown in Fig. 29.6 for both determinations of the solar abundances. As before, the older one results in a model closer to the seismic results, even if the reasons for this good agreement are not clear. The uncertainty of the seismic sound speed is below 0.002 for $r/R_\odot$ between 0.2 and 0.7. Towards the centre it is increasing due to the small number of modes extending into the core, and in the outermost layers it is larger because of the uncertainties concerning the damping of oscillations in the atmosphere. Therefore the only significant deviation of the solar model sound speed profile from the seismically determined one is the maximum of the grey line just below the convective envelope.

Although the discrepancy between model and seismic data appears to be large for the alternative model, one should keep in mind that the agreement is still within one per cent everywhere. Ignoring the effect of diffusion in the solar model calculation, which, when looking at its effect in Fig. 29.3, appears to be rather small, would result in a very similar discrepancy between model and seismic result. Overall, helioseismology confirms that stellar evolution theory can reproduce the structure of the Sun with an accuracy that is much higher than usually found in astrophysical situations.

29.5 Solar Neutrinos

Some of the nuclear reactions of the *pp* chain, as well as of the CNO cycle, produce neutrinos (Sect. 18.5.1). In addition, there are also neutrinos due to the very rare *pep* and *hep* reactions

$$
\begin{aligned}
{}^1\mathrm{H} + {}^1\mathrm{H} + e^- &\rightarrow {}^2\mathrm{H} + \nu \ (pep) \\
{}^3\mathrm{He} + {}^1\mathrm{H} &\rightarrow {}^4\mathrm{He} + e^+ + \nu \ (hep),
\end{aligned} \tag{29.1}
$$

the latter one being the trivial way to produce ^{4}He after the reactions of (18.61), but it is occurring in only 10^{-8} of all cases. However, the energy of the emitted neutrino is close to 10 MeV, and it is therefore necessary to consider this reaction. As already discussed in Sect. 18.7, the neutrinos leave the star practically without interacting with the stellar matter. The energy spectrum of neutrinos from β decay is continuous, since the electrons can take part of the energy away, while neutrinos released after an inverse β decay are essentially monochromatic. Therefore most reactions of the *pp* chain have a continuous spectrum, while the *pep*-reaction (29.1) and the electron capture on ^{7}Be (18.62) have a line spectrum. Since ^{7}Be can decay into ^{7}Li either in the ground state or in an excited state, this reaction gives two spectral lines. The neutrino spectrum of the Sun as predicted from the reactions of the *pp* chain, computed from our standard solar model, is given in Fig. 29.7. In order to obtain the neutrino spectrum of the present Sun one cannot use the simple (equilibrium) formulae (18.63) and (18.65), but must compute the rates of all the single reactions given in (18.62), (18.64) and in addition the reactions of (29.1) in a nuclear network.

Since the solar neutrinos can leave the Sun almost unimpeded they can in principle be measured in terrestrial laboratories and thus be used to learn directly about conditions in the innermost solar core. This difficult task indeed has been undertaken since 1964, when John Bahcall and Raymond Davies began to plan for an underground neutrino detector in a mine in Homestead, North Dakota. Forty years later the experiments finally have confirmed the standard solar model, and R. Davies received the Nobel Prize for his work. The time in between, however, was characterized by the "solar neutrino problem". The history of solar neutrino physics and the resolution of the problem is summarized in detail in Chap. 18 of the textbook by Weiss et al. (2004) and in Bahcall and Davies (2000).[1]

The solar neutrino problem consisted in the fact that since the first results from the so-called *chlorine* experiment by Davies there was a lack of neutrinos compared to solar model predictions. The chlorine experiment is sensitive to neutrinos with energies above 0.814 MeV and therefore, as can be seen in Fig. 29.7 mainly to the ^{8}B neutrinos, with some contribution from *pep*, *hep*, and ^{7}Be neutrinos. The experiment is based on the reaction $^{37}\mathrm{Cl} + \nu \rightarrow {}^{37}\mathrm{Ar}$, where the decays of radioactive argon nuclei are counted. The rate of neutrino captures is commonly measured in *solar neutrino units* (SNU). One SNU corresponds to 10^{-36} captures per second and per target nucleus. The predicted counts amount to 7.5 SNU for the chlorine experiment, the measurements averaged over several decades to only 2.5 ± 0.2 SNU. The deficit could indicate that the solar centre is cooler than in the models.

[1]There is also a review by Bahcall (*Solving the Mystery of the Missing Neutrinos*) at the electronic library of the Nobel prize committee (URL: `nobelprize.org/nobel_prizes/physics/articles/bahcall`).

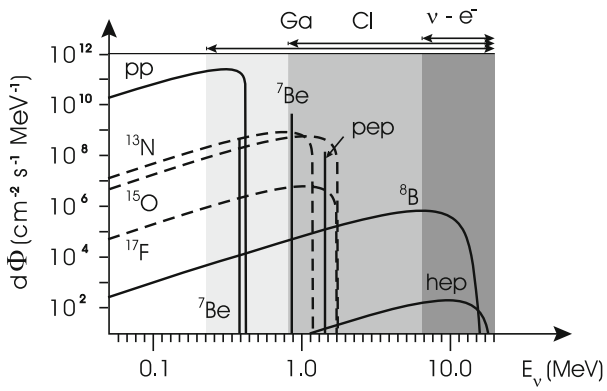

Fig. 29.7. The neutrino spectrum of the Sun as predicted from the theoretical standard solar model. The *solid lines* belong to reactions of the *pp* chain while the *broken lines* are due to reactions of the CNO cycle. The neutrinos from most of the reactions have continuous spectra, while monoenergetic neutrinos come from ^{7}Be and from the *pep*-reaction (29.1). The flux ϕ for the continuum sources is given in $\mathrm{cm}^{-2}\,\mathrm{s}^{-1}\,\mathrm{MeV}^{-1}$ and for the line sources in $\mathrm{cm}^{-2}\,\mathrm{s}^{-1}$. The sensitivity of the three types of neutrino experiments is indicated above the figure and by the *shaded* regions

To improve the experimental evidence, additional experiments were started. First, another kind of radiochemical detector using gallium in the detector fluid measured, due to a much lower energy threshold, the majority of neutrinos, including those from the *pp*-reaction. Later, electron-scattering detectors were developed, which are sensitive to the highest energies only, but which provide directional information about the neutrino source (For these detectors the *hep*-neutrinos of (29.1) have to be taken into account.). All experiments confirmed that the solar neutrino flux was of the right order of magnitude, and therefore that indeed the Sun shines by the nuclear fusion of hydrogen, but they also consistently measured a deficit of neutrinos. This deficit, however, varied between different kinds of detectors.

The various ideas on how to solve the solar neutrino problem are discussed in Chap. 18 of Weiss et al. (2004). With more and more experimental data it became evident that even hypothetical changes to the solar centre cannot solve the problem and that the solution is most likely to be found in the properties of neutrinos. All nuclear reactions emit *electron neutrinos*, and these are the only ones that were measured in terrestrial experiment, with the exception of the electron-scattering *Sudbury Neutrino Observatory* experiment in Canada, where heavy water (with a high percentage of deuterium isotopes) was used as the detector. Here also reactions with the two other types (*flavours*) of neutrinos, *muon* and *tau neutrinos* can be detected. Summing these and the *electron neutrinos* up, the total number of detections is completely consistent with the solar model prediction, within a few per cent. What created the apparent solar neutrino deficit is the fact that neutrinos can change their flavour, both while travelling through vacuum and more efficiently in the presence of electrons in

the solar interior. A similar effect was also confirmed for muon neutrinos arising in the Earth's upper atmosphere from high-energy cosmic radiation, when measured before or after they have travelled through the Earth's interior. The modelling of the solar interior, together with sophisticated experiments, has therefore resulted in new knowledge about fundamental properties of neutrinos. In particular, these so-called *neutrino oscillations* are possible only if neutrinos have mass.